Intrinsic ferromagnetism in atomically thin two-dimensional organic-inorganic van der Waals crystals

Dipayan Sen,[1] Gour Jana,[2] Nitin Kaushal,[3,4] Anamitra Mukherjee,[2] and Tanusri Saha-Dasgupta[5,*]

[1]*Department of Physics, University of Calcutta, Kolkata, West Bengal 700009, India*
[2]*School of Physical Sciences, National Institute of Science Education and Research, HBNI, Jatni 752050, India*
[3]*Department of Physics and Astronomy, The University of Tennessee, Knoxville, Tennessee 37996, USA*
[4]*Materials Science and Technology Division, Oak Ridge National Laboratory, Oak Ridge, Tennessee 37831, USA*
[5]*S. N. Bose National Centre for Basic Sciences, JD Block, Sector III, Salt Lake, Kolkata, West Bengal 700106, India*

(Received 14 April 2020; revised 5 June 2020; accepted 21 July 2020; published 5 August 2020)

Following the recent excitement in two-dimensional (2D) magnetism, we propose a yet-unexplored class of 2D ferromagnets derived out of Cr-based organic-inorganic layered compounds. Our density functional study in conjunction with model calculation establishes that assisted by the finite magnetocrystalline anisotropy, the ferromagnetic long-range order survives at the atomically thin limit consisting of monolayer of Cr spins, with calculated magnetic transition temperatures of ∼10–20-K. Upon application of modest magnetic field, the magnetic transition temperature is found to increase substantially. The calculated exfoliation energy suggests that synthesis of these 2D compounds through mechanical exfoliation is possible, which should encourage future experiments on this proposed class of 2D magnets.

DOI: 10.1103/PhysRevB.102.054411

I. INTRODUCTION

Engineering two-dimensional (2D) functional devices is an upcoming branch of technology. Extraordinary electronic properties of several 2D materials such as graphene and transition metal dichalcogenides have already been exploited in a host of electronic and optoelectronic applications [1–3]. Two-dimensional spintronics, on the other hand, remain relatively less explored, although it has drawn the attention of several researchers recently. An attempt has been made to engineer magnetism in 2D materials externally through, e.g., the introduction of defects [4–6], grain boundary and edge geometry tailoring [7], and proximity effects to magnetic substrates [8]. These efforts, however, have been found to fall short of the consistent stabilization of long-range magnetic order that is necessary for the manifestation of macroscopic magnetic effects. Successful realization of long-range magnetism, especially ferromagnetism in 2D systems, could provide breakthroughs in several frontier technologies in light of their attractive electronic and optical properties. For concise reviews on this topic, see Refs. [9–13].

A fundamental hindrance in realizing functional 2D magnetic devices is given by the Mermin-Wagner theorem [14]. This proves that a 2D array of spins, described by an underlying isotropic Heisenberg Hamiltonian, cannot show a transition to a magnetically ordered state above absolute zero temperature, with long-range ordering being destroyed by any finite thermal fluctuation. Introduction of anisotropy makes the transition temperature finite by opening a gap in the spin-wave spectrum, thus suppressing the effect of thermal fluctuations. Hence, to stabilize long-range magnetic order in 2D materials, one needs to search for compounds in which magnetic anisotropy is retained down to atomically thin layers.

Layered van der Waals (vdW) crystals offer a natural choice for exploration in this domain for two primary reasons: (a) the existence of three-dimensional (3D) ferromagnetic vdW compounds exhibiting easy-axis anisotropy and (b) weak interlayer binding facilitating direct mechanical exfoliation. Such a recipe has already been found to be successful in materials like $Cr_2Ge_2Te_6$ [15] and CrI_3 [16], which showed ferromagnetic ordering down to bilayer and monolayer limits, with magnetic transition temperatures of ≈ 30 and 45 K, respectively. Room-temperature magnetism in hydroxofluorographene has been discovered [17,18]. It remains to be seen whether this list can be expanded further by adding new candidate materials, providing an understanding of 2D ferromagnetism in a diverse class of materials.

Ternary chromium halides A_2CrX_4 ($A = Cs^+$, Rb^+, K^+, $X = Cl$) have been studied heavily, as they form rare examples of ionic insulators which show long-range ferromagnetic order, with magnetic transition temperatures around 50 K (e.g., for Rb_2CrCl_4, $T_c = 52.4$ K) [19,20]. They crystallize in the K_2NiF_4 structure, which is the $n = 1$ limit of the Ruddlesden-Popper series, $A_{n+1}M_nX_{3n+1}$. Interestingly, it has been possible to replace A in A_2CrX_4 by a variety of organic cations. To date, several such compounds with the general formula $(R\text{-}NH_3)_2MX_4$ ($R = n$-alkyl, C_nH_{2n+1} or $C_6H_5CH_2$) have been synthesized, namely, $(CH_3\text{-}NH_3)_2CrCl_4$ [21], $(C_2H_5\text{-}NH_3)_2CrCl_4$ [21], $(C_3H_7\text{-}NH_3)_2CrCl_4$ [22], $(C_6H_5\text{-}CH_2\text{-}NH_3)_2CrCl_4$ [23], $(C_6H_5\text{-}CH_2\text{-}NH_3)_2CrBr_4$ [24], and $(NH_3\text{-}(CH_2)_3\text{-}NH_3)CrCl_4$ [25]. The presence of an organic cation in the structure provides the flexibility to

*t.sahadasgupta@gmail.com

 ©2020 American Physical Society

modulate the distance between inorganic layers by considering large and complex organic cations as well as introducing van der Waals interaction between the organic chains. This gives us the hope of realizing freestanding monolayers of $(R\text{-}NH_3)_2CrX_4$ complexes, holding the promise of 2D magnetism.

In the following we explore this possibility by considering the cases of the phenylmethylamine chromium compound with Br halide, $(C_6H_5\text{-}CH_2\text{-}NH_3)_2CrBr_4$ (PMA), and the propane-1,3-diammonium chromium compound with Cl halide $(NH_3\text{-}(CH_2)_3\text{-}NH_3)CrCl_4$ (PDA), and investigating the magnetic properties of the atomically thin 2D limits of their 3D counterparts. Our choice of compounds has been guided by the availability of x-ray single-crystal studies [24,25]. Our first-principles density functional theory (DFT) based study combined with the solution of the model Hamiltonian concludes that the atomically thin 2D limit of chromium-based organic-inorganic hybrid perovskites indeed can support long-range ferromagnetic ordering, opening the door for a new family of 2D ferromagnets.

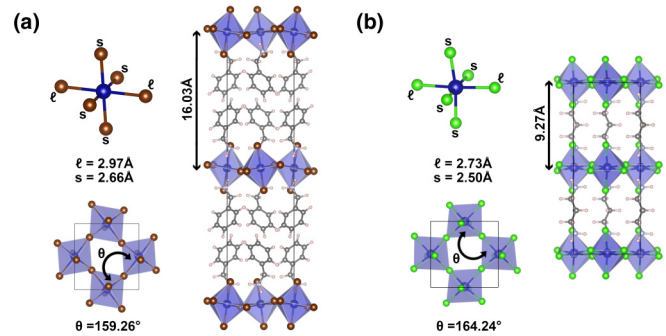

FIG. 1. Bulk crystal structures of (a) $(PMA\text{-}NH_3)_2CrBr_4$ and (b) $(NH_3\text{-}PDA\text{-}NH_3)CrCl_4$. Shown are the CrX_4 octahedron with four short (s) and two long (l) bonds, the two-dimensional connectivity of the corner-shared CrX_4 octahedra, and the 3D structure formed 2D inorganic layers connected by organic linkers. The Cr, Br, Cl, C, N, and H atoms are marked with blue, brown, green, dark gray, light gray, and white balls, respectively.

II. METHOD

The first-principles DFT calculations are performed using the Vienna *Ab initio* Simulation Package (VASP) [26–29] with the plane-wave basis and projector augmented-wave [30,31] potentials. The exchange-correlation functional is approximated within the generalized gradient approximation (GGA) as implemented in the Perdew-Burke-Ernzerhof [32] functional. The electron-electron correlation beyond the level of GGA is taken into account through a supplemented U, J_H correction at Cr sites as in Dudarev's GGA + U formalism [33]. Within the GGA + U formulation of Dudarev *et al.* [33], $U - J_H$ is a parameter of the theory for which a choice needs to be made. The localized character of Cr d states, as presented in the following, suggests the $U - J_H$ value is large. The constraint local-density approximation calculation carried out on early transition metal oxides [34] estimated a U value of 8.8 eV, while that using the linear response on a Cr-based metal-organic molecule [35] estimated a value of 6.1 eV. The estimate of U depends on the crystal environment, as the same ion in a different crystal environment may exhibit different U values due to the differential screening effect. To appreciate the U dependency on calculated magnetic properties like exchanges, we consider results for the choice of $U - J_H = 0$, 4, and 8 eV, among which 8 eV appears to be the best (see the discussion below). To resolve this issue further, we carry out a constrained DFT calculation [36] for the representative PMA compound. This calculation results in a U value of 8.7 eV with a J_H of 0.9 eV, confirming the choice of $U - J_H = 8$ eV to be not an unreasonable choice. The results presented in the following are for the choice of $U - J_H = 8$ eV, although for comparison results for $U - J_H = 4$ eV are also presented. Van der Waals interactions, important for organic ligands, are included within the modified dispersion correction DFT-D3 approach of Grimme [37]. The results are cross-checked using nonempirical vdW, available in VASP [38]. A plane-wave energy cutoff of 600 eV and Brillouin zone sampling with 10 × 2 × 10 Monkhorst-Pack grids are found to be sufficient for the convergence of energies and forces. For structural relaxations, the ions are allowed to relax until the atomic forces become less than 0.0001 eV/A. The bulk crystal structures are optimized by fixing the experimentally determined space group symmetries and experimental values of lattice parameters [a = 7.91 (7.24) Å, b = 32.06 (18.54) Å, and c = 7.76 (7.52) Å for PMA (PDA)][24,25]. Allowing lattice parameters to relax resulted in less than 2% variation of the lattice parameters compared to experimental values. A comparison of the fully relaxed crystal structures and experimentally reported ones is presented in the Appendix. Note that experimentally reported crystal structures do not include the H atom positions, which have been found theoretically. For 2D structures, the in-plane lattice constants are kept fixed as in 3D structures.

III. CRYSTAL STRUCTURE

Both the PMA and PDA compounds crystallize in the orthorhombic space group, with symmetries *Pnma* and *Pacb*, respectively. The basic structural unit, as shown in Fig. 1, is the CrX_6 octahedra with four short (s) bonds and two semicoordinated long (l) bonds due to Jahn-Teller activity of the Cr^{2+} d^4 ion. The CrX_6 octahedra corner share to give rise to two-dimensional connectivity of the inorganic part of the structure. The ammonium head group of $(RNH_3)^+$ cations form hydrogen bonding with the halogen atoms in the cavity formed by two neighboring CrX_6 octahedra. This breaks the fourfold symmetry of the parent K_2NiF_4 structure. The inorganic layer is puckered, with Cr-X-Cr bond angle deviating from 180°, with the deviation being about 15°–20°, as shown in Fig. 1. Successive inorganic layers are linked by $(RNH_3)^+$ chains, thereby separating them by about 16 Å for PMA and by about 9 Å for PDA. The organic layers are placed tail to tail and bound together solely by van der Waals forces, forming the 3D connectivity.

Starting from such layered 3D structures, it should be possible to realize the 2D $(R\text{-}NH_3)_2CrX_4/(NH_3\text{-}R\text{-}NH_3)CrX_4$ analogs through mechanical exfoliation. For mechanical exfoliation, it is necessary to overcome an energy barrier, namely, the cleavage energy E_{cl}. This can be defined as the energy needed to create two (top and bottom) surfaces by

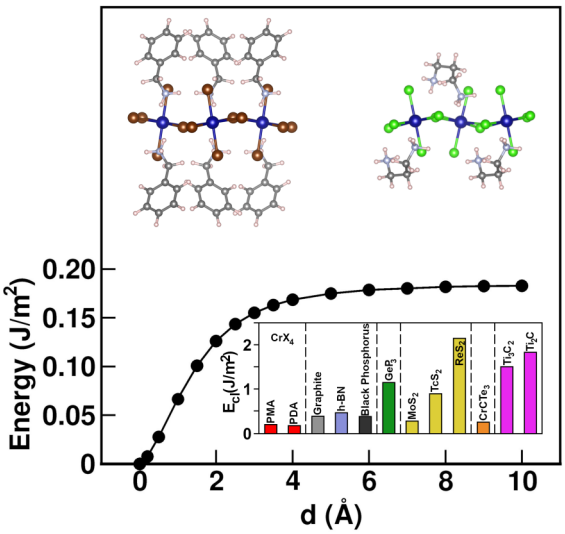

FIG. 2. Energy difference between layer-separated and bulk compounds as a function of interlayer separation d. Shown for the representative case of PMA. Similar results are obtained for PDA. The bottom inset shows a comparison of cleavage energy for PMA and PDA compounds in comparison to other layered compounds. The data for graphite, h-BN, black phosphorus, GeP_3, MoS_2, TcS_2, ReS_2, $CrCTe_3$, Ti_3C_2, and Ti_2C are obtained from Refs. [41–48], respectively. Two top insets show the 2D structures of PMA and PDA. The Cr, Br, Cl, C, N, and H atoms are marked with blue, brown, green, dark gray, light gray, and white balls, respectively.

cleaving the bulk compounds along the inorganic CrX_4 plane [39,40], $E_{cl} = 2\frac{(E_{\text{slab}} - E_{\text{bulk}})}{2A}$, where E_{slab} is the total energy of the cleaved system with two bare surfaces, E_{bulk} is the total energy of the same in the bulk state, and A is the surface area. Figure 2 shows the estimated cleavage energies for PMA and PDA, obtained by computing the area-normalized energy differences between the layer-separated and bulk compounds upon increasing the interlayer separation until the individual layers are sufficiently far that the dispersive interactions are negligible. It is encouraging to note that computed E_{cl} values (0.182 and 0.175 J/m^2 for PMA and PDA, respectively) are smaller than those of the layered compounds reported earlier (see the inset in Fig. 2) and, by about a factor of 2, smaller than the experimentally measured cleavage energy of graphite (0.37 J/m^2) [41]. This strongly suggests that these layered compounds should be cleavable.

The derived 2D structures are shown as insets in Fig. 2. Compared to the bulk counterparts, the Cr-X-Cr buckling angles were found to deviate by 1°–5°, with the overall connectivity in the inorganic plane and Cr-X bond lengths remaining more or less unchanged.

IV. ELECTRONIC STRUCTURE

The calculated GGA + U density of states of bulk PMA and PDA and their 2D counterparts, projected to Cr d, X (Cl/Br) p, and ligand states, is shown in Fig. 3. As seen from the figure, Cr d states are completely empty in the minority-spin channel, which is suggestive of the high-spin configuration of Cr^{2+}. In the majority-spin channel, the Cr d states are primarily occupied, spanning an energy range

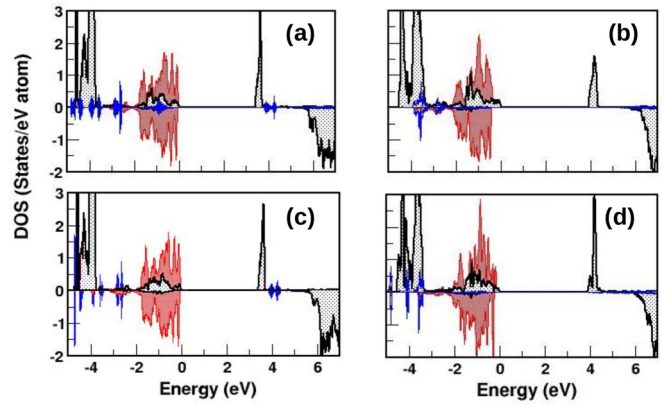

FIG. 3. The GGA + U density of states, projected to Cr d (black), halogen p [red (light grey)], and organic ligand states [blue (dark grey)] for (a) 3D-PMA, (b) 3D-PDA, (c) 2D-PMA, and (d) 2D-PDA. The zero of the energy is set at the Fermi energy.

of about −4.5 eV to about −3.5 eV, with an unoccupied part around 3.5 or 4 eV, in agreement with the high-spin d^4 configuration of Cr. The halogen states occupy an energy range −2 to 0 eV, admixed with Cr d states. The states arising from organic ligands lie around −3 eV. The overall features of the DOS do not show a significant difference between the 3D and 2D counterparts.

The GGA + U scheme results in a magnetic moment of about 3.8μ_B at the Cr site, with a total moment of 16μ_B in the cell, in accordance with the four formula unit cell of the orthorhombic symmetry with four Cr atoms in the cell. A significant fraction of the moment is found to reside at halogen sites, implying strong Cr-X covalency.

V. MAGNETIC PROPERTIES

The magnetic exchanges of the considered (PMA-NH_3)$_2$CrBr$_4$ and (NH_3-PDA-NH_3)CrCl$_4$ compounds are estimated by computing total energies of four ordered arrangements of the Cr^{2+} $S = 2$ spins: (a) ferromagnetic (FM), (b) A-type antiferromagnetic (A-AFM), where Cr^{2+} spins align parallelly within the plane and antiparallelly out of the plane, (c) C-type antiferromagnetic (C-AFM), where Cr^{2+} spins align antiparallelly in the plane and parallelly out of the plane, and (d) G-type antiferromagnetic (G-AFM), where Cr^{2+} spins align antiparallelly in all directions and map onto an effective spin model with nearest-neighbor in-plane interaction and out-of-plane interaction. Farther-neighbor interactions are negligibly small due to large distances and/or the absence of connected paths. For example, for PMA, second-neighbor intralayer exchange interactions do not have connected superexchange paths and have a distance of 7.76 Å compared to 5.54 Å for nearest neighbors. This is also in accordance with experimental findings on these compounds for the bulk structure [49]. For their 2D counterparts, two ordered spin states of the Cr^{2+} ion were considered: (a) FM and (b) AFM, where Cr^{2+} spins aligned antiparallelly within the plane. The computed GGA + U energies are given in Table I.

The resultant magnetic exchanges, obtained by mapping the total energies onto the $S = 2$ spin model $H =$

TABLE I. Total energy of 3D and 2D structures of the considered organic-inorganic compounds in different magnetic configurations of four (two) Cu spins in the 3D (2D) unit cell. Magnetic configurations are specified by + (−) signs for spin-up (spin-down) states of the Cr ions, with the first two Cr spins in the same plane and the next two in the neighboring plane in three dimensions. The two Cu spins in two dimensions lie in same plane. The energy is measured with respect to the FM configuration.

Systems	Magnetic states	Energy (meV)
PMA-3D	FM (+ + + +)	0
	A-AFM (+ + − −)	−0.162
	C-AFM (+ − + −)	50.737
	G-AFM (+ − − +)	48.927
PMA-2D	FM (+ +)	0
	AFM (+−)	23.940
PDA-3D	FM (+ + ++)	0
	A-AFM (+ + − −)	−0.246
	C-AFM (+ − + −)	48.895
	G-AFM (+ − − +)	43.631
PDA-2D	FM (+ +)	0
	AFM (+−)	19.589

$\sum_{\langle ij\rangle} J_{ij}\mathbf{S}_i.\mathbf{S}_j$ ($\mathbf{S}_i$ is the spin operator at site i, with $\langle ij\rangle$ denoting nearest neighbors, $J<0$ indicates FM exchange, and $J>0$ indicates AFM exchange), for the 3D and 2D counterparts are shown in Fig. 4(a). We find the in-plane exchanges are ferromagnetic for both the 3D and 2D counterparts, with estimated values of about 0.8 meV for the choice of $U-J_H = 8$ eV. The influence of the choice of the $U-J_H$ value on exchanges can be appreciated by

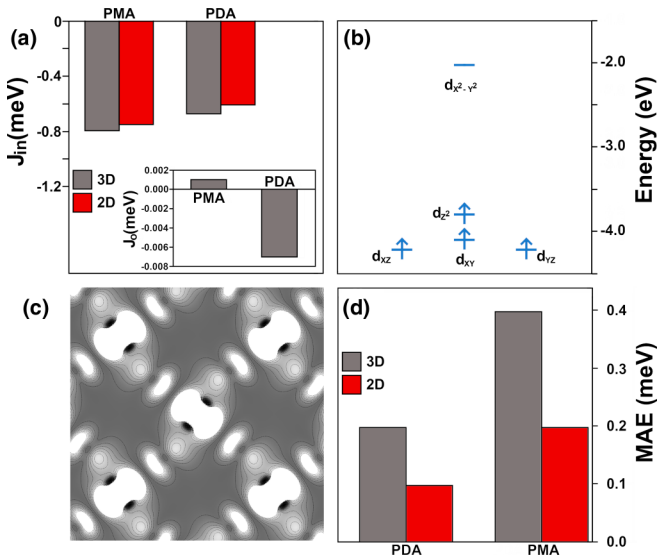

FIG. 4. (a) In-plane exchanges J_{in} of $(PMA\text{-}NH_3)_2CrBr_4$ and $(NH_3\text{-}PDA\text{-}NH_3)CrCl_4$ in the 3D bulk structure and 2D counterparts. The inset shows the out-of-plane exchange J_o in 3D structures. (b) The crystal field splitting and occupancy of the Cr^{2+} ion. (c) A plot of spin density showing orbital ordering due to antiferrodistortive distortion. (d) Calculated magnetic anisotropy energy of $(PMA\text{-}NH_3)_2CrBr_4$ and $(NH_3\text{-}PDA\text{-}NH_3)CrCl_4$ in the 3D bulk structure and 2D counterparts.

comparing the J values obtained with the choice of $U-J_H = 4$ eV, which are $J_{in} \sim -2$ meV for PMA and -1.80 meV for PDA, and the corresponding values for $U-J_H = 0$ eV, which are -8.8 meV and -8.2 meV, respectively. The agreement between the calculated and measured values of near-neighbor ferromagnetic exchange (13.1 K) extracted by high-temperature series expansion fits of the magnetic susceptibility [50] for the PMA compound is found to be best for the choice of $U-J_H = 8$ eV among the three choices 0 eV ($J = 102$ K), 4 eV ($J = 23$ K), and 8 eV ($J = 9.3$ K). The agreement is good, considering the limitations of the theory and the fitting procedure of the experiments as well as sample qualities. We have also checked the results for magnetic exchanges by using the crystal structure from the full structural relaxation and found the influence to be not significant, resulting in $J = 0.76$ meV with a fully optimized structure, compared to 0.8 meV in the PMA compound. For 3D systems, the out-of-plane exchanges are two orders of magnitude smaller than the in-plane exchanges, in accordance with the large separation between the layers connected through weak van der Waals coupling.

The in-plane ferromagnetic exchange is driven by the antiferrodistortive ordering of the Jahn-Teller distorted CrX_6, which makes tetragonally elongated CrX_6 octahedra lie in plane, but the local z axes of the neighboring CrX_6 octahedra are at right angles to one another. The tetragonal crystal field splits the e_g levels with $d_{3z^2-r^2}$ being half filled and $d_{x^2-y^2}$ being empty, with a large energy separation of about 1.7 eV [see Fig. 4(b)], with z being the local coordinate pointed along the direction of elongation. The antiferrodistortive structure makes the half-filled $d_{3z^2-r^2}$ orbital at a given Cr site, delocalized to X 3 p_z due to the finite Cr-X covalency, overlap with the empty $d_{x^2-y^2}$ orbital at the neighboring site [see Fig. 4(c)], promoting ferromagnetic Cr-X-Cr superexchange.

Having estimated magnetic exchanges, we next compute the magnetic anisotropy energy (MAE), which is crucial for the stabilization of long-range magnetic order in the 2D limit. MAEs are estimated from fully self-consistent total-energy calculations, switching on the spin-orbit coupling (SOC) within the framework of GGA + U + SOC calculations with the magnetization axis pointed along the c axis and perpendicular to it. The easy-axis magnetic anisotropy energy is found to be slightly smaller in the 2D counterparts compared to bulk compounds, with a finite nonzero value of 0.2 meV for PMA and 0.1 meV for PDA [see Fig. 4(d)]. While the MAE values are small, pushing to the limit of DFT accuracy, similarly small values of MAE have been estimated for $Cr_2Ge_2Te_6$ [15].

VI. SPIN-WAVE SPECTRUM

The magnetic behavior of the derived 2D structures can be described by an $S = 2$ Heisenberg Hamiltonian with generalized magnetic anisotropy:

$$H = J\sum_{\langle ij\rangle} S_i \cdot S_j + \sum_i A_{i\alpha,\beta} S_{i\alpha} S_{i\beta},$$

where $A_{i\alpha,\beta}$ is a matrix with real diagonal components and complex off-diagonal terms and encodes all possible ways in which the single-ion anisotropy can be added to the Hamiltonian. J is assumed to be ferromagnetic (negative) following

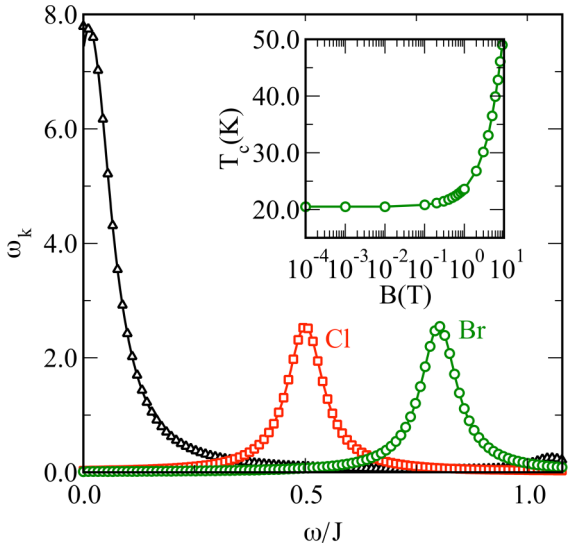

FIG. 5. The spin-wave spectra obtained by exact diagonalization of the spin Hamiltonian, setting the anisotropy to zero (black), to values corresponding to PDA (red), and to values corresponding to PMA (green). The system size is 4×4. The inset shows the dependence of T_c of PMA on the external magnetic field. It is estimated from renormalized spin-wave theory, as discussed in the text.

the DFT input. Within the framework of the general form of the easy-axis single-ion anisotropy (SIA), several possibilities exist. In the simplest possibility, which is also conventionally used, A_{izz} is the only nonzero element of $A_{i\alpha,\beta}$. This leads to $-A_{izz}S_{iz}^2$, as the SIA term in the Hamiltonian at site i, favoring orientation along the z axis. For the DFT estimate of the SIA energy Δ_{Cr}, this would mean that we identify $A_{izz} = |\Delta_{\mathrm{Cr}}|$ and assume it is the same on all sites. With this choice, exploiting the large value of the spin and employing the $1/S$ Holstein-Primakoff approach with $S_i^+ = (2S - n_i)^{1/2}a_i$, $S_i^- = a^\dagger(2S - n_i)^{1/2}$, and $S_i^z = S - n_i$ [a_i ($a_i^\dagger$) are magnon (annihilation) creation operators, and n_i are the boson occupation at site i], the spin-wave dispersion is given as

$$\omega_k = S\{J[4 - 2\cos(k_x) - 2\cos(k_y)]\} + |\Delta_{Cr}|(2S - 1).$$

In the limit of $|k| \to 0$, $\omega_k \approx S|J||k^2| + \Delta_{Cr}(2S - 1)$. Thus, the gap in the spin-wave spectra is $3\Delta_{Cr}$, with $S = 2$. As is well known, the gap to the spin-wave excitation avoids the infrared divergence of the magnon density at low temperatures and the ensuing collapse of long-range order that would have otherwise occurred in the two-dimensional Heisenberg model.

Moving beyond the $T = 0$ Holstein-Primakoff approach, we compute the spin-wave spectrum within Lanczos-based diagonalization, considering the $A_{izz}S_{iz}^2$ term. The results are shown in Fig. 5 (main panel). As expected in the absence of anisotropy ($\Delta = 0$), the spin-wave spectrum shows the absence of a gap. Inclusion of anisotropy gives rise to a nonzero excitation gap in the spectrum, thus stabilizing the spontaneous symmetry-breaking long-range ferromagnetic ordering. With DFT-estimated parameters J and Δ, the spin-wave gap for PDA turns out to be 0.3 meV, while for PMA the gap is estimated to be 0.6 meV. These values are in close agreement with the Holstein-Primakoff estimate of $-A_{izz}(2S - 1)$, which gives 0.08 meV (PMA) and 0.18 meV (PDA) for $A_{izz} = |\Delta_{Cr}|$ and $|\Delta_{\mathrm{Br}}|$, respectively.

To estimate T_c for these materials, we have employed renormalized spin-wave theory [51,52], which was used recently in a similar context [15]. In this approach, we estimate the number density of magnons (bosons) at a given temperature by computing the temperature-dependent magnon occupation. To do this we first use a self-consistent Hartree-Fock scheme to calculate the magnon dispersion $\tilde{\omega}_{\mathbf{q}}$, retaining the magnon-magnon interaction term. From the magnon number density we calculate

$$M(T)/M(0) \equiv 1 - \frac{1}{NS}\sum_{\mathbf{q}} \frac{1}{e^{\hbar\tilde{\omega}_{\mathbf{q}}/K_BT} - 1}.$$

Here, $M(T)/M(0)$ is the ratio of the temperature-dependent magnetization at a temperature T to the saturation magnetization at $T = 0$. K_B is the Boltzmann constant, and N is the total number of lattice sites. An estimate of T_c can be made from this by identifying the T_c with the temperature where $M(T)/M(0)$ becomes zero. For the cases of PMA and PDA, we find that the finite anisotropy stabilizes a T_c of 21 and 11 K, respectively. We emphasize that similar to monolayer CrI_3 [16], in the studied compounds, even the zero-field case shows a substantial value of T_c. For comparison, T_c values calculated for bulk PMA and PDA compounds turn out to be 37 and 18 K, respectively. To investigate the effect of the choice of $U - J_H$ on T_c, T_c values are also calculated using J estimated for $U - J_H = 4$ eV, resulting in estimated T_c of 23 and 14 K for 2D PMA and PDA, respectively, and those of bulk compounds of 40 K (PMA) and 22 K (PDA). The only experimentally estimated T_c available for bulk PMA is 52 K [50]. Considering the approximations related to renormalized spin-wave theory as well as estimates of U-dependent J and anisotropy energies, the comparison of calculated T_c of bulk and experimental estimates is reasonable. We note that T_c of the 2D counterparts are 0.5–0.6 times that of the bulk counterpart. For monolayer CrI_3 and bilayer $Cr_2Ge_2Te_6$, the ratio was found to be about 0.75 and about 0.4, respectively [53].

Further, we explore the effect of magnetic field. Application of a modest strength of the magnetic field is found to enhance T_c significantly (see the inset in Fig. 5), with a value of ~31 K at a field of 3 T for PMA. A similar trend was found in $Cr_2Ge_2Te_6$ [15].

VII. SUMMARY

In summary, employing first-principles DFT calculations, the solution of the DFT-derived spin Hamiltonian from spin-wave theory, and exact diagonalization, we explored the possibility of 2D ferromagnetism in Cr-based organic-inorganic hybrid compounds. Our computational study showed these compounds are easily exfoliable due to the weak van der Waals interactions between organic tails, with the exfoliation energy being smaller than those of graphite, metal dichalcogenides, and h-BN. The exfoliated 2D counterparts retain the ferromagnetic correlation between the in-plane Cr spins arising due to the antiferrodistortive arrangement of the Cr-halogen octahedra. Interestingly, the easy-axis anisotropy of

TABLE II. Experimental structural parameters of PMA and PDA [24,25]. Quantities in parentheses represent the corresponding values after full relaxation of the structures. H atom positions are not shown as they are not available in the literature.

System	Lattice constants (a, b, c) (Å)	Atom	Wyckoff positions	Coordinates (x, y, z)
PMA (bulk)	7.909 (7.791), 32.060 (31.997), 7.760 (7.625)	Br1	8c	0.955 (0.952), 0.421 (0.417), 0.023 (0.025)
		Br2	8c	0.783 (0.791), −0.489 (−0.488), 0.239 (0.269)
		N	8c	0.534 (0.531), −0.069 (−0.072), 0.529 (0.529)
		C1	8c	0.447 (0.440), −0.104 (−0.108), 0.450 (0.445)
		C2	8c	0.478 (0.475), −0.145 (−0.149), 0.535 (0.537)
		C3	8c	0.618 (0.622), −0.169 (−0.172), 0.500 (0.498)
		C4	8c	0.649 (0.653), −0.205 (−0.210), 0.591 (0.587)
		C5	8c	0.525 (0.539), −0.219 (−0.224), 0.702 (0.717)
		C6	8c	0.397 (0.393), −0.197 (−0.200), 0.750 (0.757)
		C7	8c	0.368 (0.361), −0.159 (−0.163), 0.659 (0.666)
		Cr	4b	0.000 (0.000), −0.500 (−0.500), −0.000 (0.000)
PDA (bulk)	7.235 (7.103), 18.535 (18.432), 7.517 (7.392)	Cl1	8d	0.978 (0.975), 0.870 (0.865), 0.960 (0.958)
		Cl2	8d	0.245 (0.251), 0.017 (0.016), 0.212 (0.222)
		N	8d	0.014 (0.012), 0.378 (0.381), 0.546 (0.551)
		C1	8d	0.973 (0.982), 0.312 (0.315), 0.441 (0.423)
		C2	4c	0.032 (0.030), 0.250 (0.250), 0.527 (0.525)
		Cr	4a	0.000 (0.000), 0.000 (0.000), 0.000 (0.000)

Cr spins, although showing a slight decrease in 2D systems compared to the corresponding 3D counterparts, remains finite with appreciable values of 0.1–0.2 meV. This helps in the stabilization of the ferromagnetic long-range order in the 2D monolayer of Cr spins. The calculated T_c values, which depend on the choice of the U parameter in our theory, turn out to be 21–23 and 11–14 K for the PMA and PDA compounds, respectively, the two Cr-based organic-inorganic compounds considered in the present study. Compared to calculated bulk T_c, the corresponding monolayer T_c is suppressed but remains substantial. The trend of T_c being lower for the Cl compound (PDA) compared to the Br compound (PMA) follows the trend observed for related bulk compounds [24]. We further found that application of a modest magnetic field is capable of enhancing T_c, as found for the case of $Cr_2Ge_2Te_6$ [15]. In the case of PMA, upon application of magnetic field, T_c is found to be enhanced appreciably, giving a T_c which is in the same ballpark as other insulating 2D ferromagnets like CrI_3, with an experimentally estimated value of 45 K in monolayer CrI_3 [16]. We expect our theoretical exercise will motivate future experimental studies.

ACKNOWLEDGMENTS

T.S.-D. thanks the Department of Science and Technology, India, for the support through the Thematic Unit of Excellence. D.S. thanks the University Grants Commission, Government of India, for providing financial support under the D. S. Kothari Post Doctoral Fellowship scheme. T.S.-D. and D.S. thank S. Bandyopadhyay for fruitful discussions.

APPENDIX: CRYSTAL STRUCTURE DATA

The structural parameters of PMA and PDA are given in Table II.

[1] C. Uthaisar and V. Barone, Nano Lett. **10**, 2838 (2010).
[2] K. F. Mak and J. Shan, Nat. Photonics **10**, 216 (2016).
[3] S. Manzeli, D. Ovchinnikov, D. Pasquier, O. V. Yazyev, and A. Kis, Nat. Rev. Mater. **2**, 17033 (2017).
[4] R. R. Nair, M. Sepioni, I.-L. Tsai, O. Lehtinen, J. Keinonen, A. V. Krasheninnikov, T. Thomson, A. K. Geim, and I. V. Grigorieva, Nat. Phys. **8**, 199 (2012).
[5] H. González-Herrero, J. M. Gómez-Rodríguez, P. Mallet, M. Moaied, J. J. Palacios, C. Salgado, M. M. Ugeda, J. Y. Veuillen, F. Yndurain, and I. Brihuega, Science **352**, 437 (2016).
[6] B. Uchoa, V. N. Kotov, N. M. R. Peres, and A. H. Castro Neto, Phys. Rev. Lett. **101**, 026805 (2008).
[7] J. Jung, T. Pereg-Barnea, and A. H. MacDonald, Phys. Rev. Lett. **102**, 227205 (2009).
[8] H. X. Yang, A. Hallal, D. Terrade, X. Waintal, S. Roche, and M. Chshiev, Phys. Rev. Lett. **110**, 046603 (2013).
[9] J. Tuček, P. Błoński, J. Ugolotti, A. K. Swain, T. Enoki, and R. Zbořil, Chem. Soc. Rev. **47**, 3899 (2018).
[10] W. Han, R. K. Kawakami, M. Gmitra, and J. Fabian, Nat. Nanotechnol. **9**, 794 (2014).
[11] E. J. Kan, Z. Y. Li, and J. L. Yang, Nano **3**, 433 (2008).
[12] W. Q. Liu and Y. B. Xu, Curr. Opin. Solid State Mater. Sci. **20**, 388 (2016).
[13] X. X. Li and J. L. Yang, Natl. Sci. Rev. **3**, 365 (2016).
[14] N. D. Mermin and H. Wagner, Phys. Rev. Lett. **17**, 1133 (1966).
[15] C. Gong, L. Li, Z. Li, H. Ji, A. Stern, Y. Xia, T. Cao, W. Bao, C. Wang, Y. Wang, Z. Q. Qiu, R. J. Cava, S. G. Louie, J. Xia, and X. Zhang, Nature (London) **546**, 265 (2017).
[16] B. Huang, G. Clark, E. Navarro-Moratalla, D. R. Klein, R. Cheng, K. L. Seyler, D. Zhong, E. Schmidgall, M. A. McGuire, D. H. Cobden, W. Yao, D. Xiao, P. Jarillo-Herrero, and X. Xu, Nature (London) **546**, 270 (2017).

[17] J. Tuček, K. Holá, G. Zoppellaro, P. Błoński, R. Langer, M. Medved, T. Susi, M. Otyepka, and R. Zbořil, ACS Nano **12**, 12847 (2018).
[18] J. Tuček, K. Holá, A. B. Bourlinos, P. Błoński, A. Bakandritsos, J. Ugolotti, M. Dubecký, F. Karlický, V. Ranc, K. Čépe, M. Otyepka, and R. Zbořil, Nat. Commun. **8**, 14525 (2017).
[19] P. Day, J. Magn. Magn. Mater. **54–57**, 1442 (1986).
[20] M. J. Fair, M. T. Hutchings, P. Day, R. Ghosh, and P. J. Walker, J. Phys. C **11**, L813 (1978).
[21] C. Bellitto and P. Day, J. Chem. Soc., Chem. Commun., 870 (1976), doi: 10.1039/C39760000870.
[22] M. J. Stead and P. Day, J. Chem. Soc., Dalton Trans., 1081 (1982), doi: 10.1039/DT9820001081.
[23] C. Bellitto and P. Day, J. Chem. Soc., Dalton Trans., 1207 (1978), doi: 10.1039/DT9780001207.
[24] D. M. Halepoto, L. F. Larkworthy, D. C. Povey, and V. Ramdas, Inorg. Chim. Acta **162**, 71 (1989).
[25] M. A. Babar, M. F. C. Ladd, L. F. Larkworthy, D. C. Povey, K. J. Proctor, and L. J. Summers, J. Chem. Soc., Chem. Commun., 1046 (1981), doi: 10.1039/C39810001046.
[26] G. Kresse and J. Hafner, Phys. Rev. B **47**, 558 (1993).
[27] G. Kresse and J. Hafner, Phys. Rev. B **49**, 14251 (1994).
[28] G. Kresse and J. Furthmüller, Comput. Mater. Sci. **6**, 15 (1996).
[29] G. Kresse and J. Furthmüller, Phys. Rev. B **54**, 11169 (1996).
[30] P. E. Blöchl, Phys. Rev. B **50**, 17953 (1994).
[31] G. Kresse and D. Joubert, Phys. Rev. B **59**, 1758 (1999).
[32] J. P. Perdew, K. Burke, and M. Ernzerhof, Phys. Rev. Lett. **77**, 3865 (1996).
[33] S. L. Dudarev, G. A. Botton, S. Y. Savrasov, C. J. Humphreys, and A. P. Sutton, Phys. Rev. B **57**, 1505 (1998).
[34] F. Aryasetiawan, K. Karlsson, O. Jepsen, and U. Schönberger, Phys. Rev. B **74**, 125106 (2006).
[35] G. W. Mann, K. Lee, M. Cococcioni, B. Smit, and J. B. Neaton, J. Chem. Phys. **144**, 174104 (2016).
[36] O. Gunnarsson, O. K. Andersen, O. Jepsen, and J. Zaanen, Phys. Rev. B **39**, 1708 (1989).
[37] S. Grimme, J. Antony, S. Ehrlich, and H. Krieg, J. Chem. Phys. **132**, 154104 (2010).
[38] K. Lee, E. D. Murray, L. Kong, B. I. Lundqvist, and D. C. Langreth, Phys. Rev. B **82**, 081101(R) (2010).
[39] R. Benedek and M. M. Thackeray, Phys. Rev. B **83**, 195439 (2011).
[40] D. Santos-Carballal, A. Roldan, R. Grau-Crespo, and N. H. de Leeuw, Phys. Chem. Chem. Phys. **16**, 21082 (2014).
[41] W. Wang, S. Dai, X. Li, J. Yang, D. J. Srolovitz, and Q. Zheng, Nat. Commun. **6**, 7853 (2015).
[42] J. H. Jung, C. H. Park, and J. Ihm, Nano Lett. **18**, 2759 (2018).
[43] Y. Jing, Y. Ma, Y. Li, and T. Heine, Nano Lett. **17**, 1833 (2017).
[44] M. A. McGuire, G. Clark, Santosh KC, W. M. Chance, G. E. Jellison, Jr., V. R. Cooper, X. Xu, and B. C. Sales, Phys. Rev. Mater. **1**, 014001 (2017).
[45] Y. Jiao, L. Zhou, F. Ma, G. Gao, L. Kou, J. Bell, S. Sanvito, and A. Du, ACS Appl. Mater. Interfaces **8**, 5385 (2016).
[46] H. Wang, E. Liu, Y. Wang, B. Wan, C. H. Ho, F. Miao, and X. G. Wan, Phys. Rev. B **96**, 165418 (2017).
[47] S. Chabungbam and P. Sen, Phys. Rev. B **96**, 045404 (2017).
[48] K. Mondal and P. Ghosh, Solid State Commun. **299**, 113657 (2019).
[49] D. B. Mitzi, Prog. Inorg. Chem. **48**, 1 (1999).
[50] C. Bellitto and P. Day, J. Mater. Chem. **2**, 265 (1992).
[51] M. Bloch, Phys. Rev. Lett. **9**, 286 (1962).
[52] K. Yosida, *Theory of Magnetism* (Springer-Verlag, Berlin, Heidelberg, 1998).
[53] M. Gibertini, M. Koperski, A. F. Morpurgo, and K. S. Novoselov, Nat. Nanotechnol. **14**, 408 (2019).